Confinement physics for thermal, neutral, high-charge-state plasmas in nested-well solenoidal traps

D. D. Dolliver and C. A. Ordonez
Department of Physics, University of North Texas, Denton, Texas 76203-5370
(Received 2 March 1998; revised manuscript received 26 January 1999)

A theoretical study is presented which indicates that it is possible to confine a neutral plasma using static electric and solenoidal magnetic fields. The plasma consists of equal temperature electrons and highly stripped ions. The solenoidal magnetic field provides radial confinement, while the electric field, which produces an axial nested-well potential profile, provides axial confinement. A self-consistent, multidimensional numerical solution for the electric potential is obtained, and a fully kinetic theoretical treatment on axial transport is used to determine an axial confinement time scale. The effect on confinement of the presence of a radial electric field is explored with the use of ion trajectory calculations. A thermal, neutral, high-charge-state plasma confined in a nested-well trap opens new possibilities for fundamental studies on plasma recombination and cross-field transport processes under highly controlled conditions. [S1063-651X(99)09006-6]

PACS number(s): 52.25.Wz, 52.55.Lf

I. INTRODUCTION

Plasma traps that use a solenoidal magnetic field for radial confinement and an electric field for axial confinement have traditionally been used to confine non-neutral plasmas consisting only of electrons or only of ions [1]. In principle, however, such traps can also be used to confine a neutral plasma. The required axial electric potential profile and electrode configuration are illustrated in Fig. 1. For obtaining a region of neutral plasma with the potential profile in Fig. 1(a), positive ions would be confined within the ''inner well'' and electrons would be confined within the ''outer well'' in such a way that the electron plasma overlaps the ion plasma. For this to occur, the electrons must have a thermal energy greater than or about equal to the increase in their potential energy between $z=z_m$ and $z=0$. (The location $z=z_m$ is defined as the location where the maximum potential occurs.) However, for the ions to remain confined, they must have a thermal energy much less than the difference in their potential energy between $z=z_m$ and $z=0$. These two conditions can be simultaneously satisfied if the temperature of the electron plasma component is much larger than that of the ion plasma component. In fact, experimental evidence indicates that it is possible to confine overlapping plasma components in this way [2]. Using the nested-well approach, simultaneous confinement of electrons and protons at widely different temperatures was achieved such that sympathetic cooling occurred between species [2]. (In Ref. [2], the electric potential profile was inverted relative to that shown in Fig. 1(a), and electrons were confined within the inner well while hotter protons were confined within the outer well.) The experimental data reported in Ref. [2] do not show that the overlap region achieved was neutral. However, theoretical analyses do support the prospect of trapping a neutral plasma within a solenoidal magnetic field using an externally applied electric field for providing axial confinement. The first self-consistent calculation of achieving simultaneous confinement and overlap of oppositely signed plasma species at widely different temperatures was presented in Ref. [3]. With the assumption of azimuthal symmetry, a three-dimensional charge density profile was obtained using a two-dimensional calculation. The charge density profile obtained clearly showed a neutral plasma overlap region.

Along with the two-temperature approach, the possibility of confining an electron plasma in a nonequilibrium plasma state which overlaps a low charge state, equal temperature ion plasma to form a neutral plasma region has been studied [4]. This approach, along with the two-temperature approach, necessarily requires a repetitive, time-dependent manipulation of the electrode voltages to counteract the effect of interparticle collisions. In the nonequilibrium approach, interparticle collisions tend to drive the electron plasma to an equilibrium plasma state while, in the two-temperature approach, collisions tend to reduce the temperature difference between the two plasma components. In the present work, the possibility of using a static electric field to provide constant axial confinement of a neutral plasma within a solenoidal magnetic field is explored. The plasma consists of highly stripped ions and equal temperature electrons. With a higher

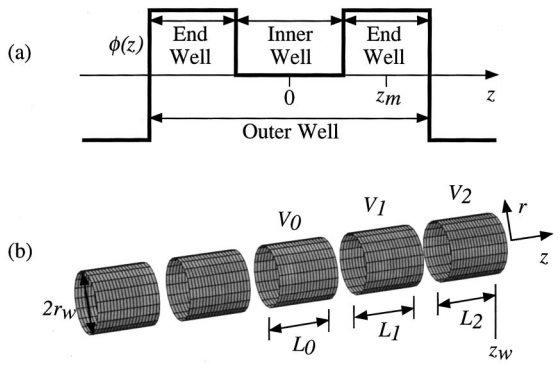

FIG. 1. The nested-well approach to plasma confinement. A nested-well electric potential profile illustrated qualitatively (a) is produced using cylindrically symmetric electrodes (b). The electrodes are aligned parallel to an externally produced solenoidal magnetic field. Under conditions described in the text, a thermal, neutral, high-charge-state plasma can be trapped within the inner well.

charge state, the ions are exposed to a larger change in potential energy between $z=0$ and $z=z_m$ relative to the electrons, and the conditions for achieving neutral plasma confinement can be met. In Sec. II, the method used to obtain a self-consistent numerical solution for the potential and charge density is described, and a calculation is presented which illustrates confinement of a near-thermal, neutral plasma consisting of electrons and high charge state ions. In Sec. III, relations describing axial confinement are derived using a fully kinetic theoretical approach, and the possibility of achieving near-perfect axial confinement is assessed. In Sec. IV, results of an ion trajectory calculation are presented which demonstrate that magnetic radial confinement is possible. Concluding remarks are found in Sec. V.

II. SELF-CONSISTENT NUMERICAL SOLUTION

Figure 1(b) shows the electrode configuration considered. The configuration has symmetry across the $z=0$ plane, as well as an azimuthal symmetry. The center electrode is held at voltage V_0. The electrodes of length L_1 are held at $V_1 > V_0$, while the outer electrodes of length L_2 are held at $V_2 < V_0$. To reduce the computation time, the electrode separations are neglected, the outer electrodes are considered to be capped on the outer ends with vertical electrode walls held at V_2, and the outer electrodes are chosen to have lengths equal to the electrode radius ($L_2 = r_w$). This computational model is expected to provide results which suitably describe a comparable open-ended plasma trap provided $L_2 \gg r_w$ for the open-ended trap.

The externally applied voltages V_1 and V_2 must be chosen so that the ions are well confined by the inner well and the electrons are well confined by the outer well. However, the electrons must also have enough thermal energy to enter the inner well. If the magnitude of the change in potential from $z=0$ to its maximum along some magnetic field line is $\Delta\phi_m$, good axial confinement of the ions along that field line occurs if $Ze\Delta\phi_m/T \gg 1$, where T is the plasma temperature in energy units, Z is the ion charge state, and e is the unit charge. For the electrons to overlap the inner well along that field line, $e\Delta\phi_m/T \lesssim 1$ must be satisfied where the electrons are assumed to have the same temperature as the ions. With $Z \gg 1$, both requirements can be met.

A finite difference algorithm is used to solve Poisson's equation. $\nabla^2\phi = -\rho/\epsilon_0$. Here, $\rho(r,z) = -en_e(r,z) + e\Sigma_z Z n_Z(r,z)$ is the charge density, ϵ_0 is the permittivity of free space, n_e is the electron density, and n_Z is the density of ions of charge state Z. n_Z is obtained using a cutoff Maxwell-Boltzmann distribution. The distribution of velocities parallel to z excludes ions which would not be axially confined,

$$f_z(r,z,v_z) = C_1 e^{-\beta_Z v_z^2 - \psi_i(r,z)} \Theta(v_{z\,\max} - |v_z|). \tag{1}$$

Here C_1 is a normalization factor, $\beta_Z = m_Z/(2T)$, $v_{z\,\max} = \sqrt{[\psi_{im}(r) - \psi_i(r,z)]/\beta_Z}$, m_Z is the ion mass, $\psi_i(r,z) = Ze\phi(r,z)/T$, and $\psi_{im}(r)$ is the maximum value of the normalized ion potential energy which occurs along a magnetic field line at r. Similarly the distribution of velocities perpendicular to z is given by

$$f_\perp(r_c, v_\perp) = C_2 v_\perp e^{-\beta_Z v_\perp^2} \Theta(v_{\perp\,\max} - v_\perp) \tag{2}$$

where $v_{\perp\,\max} = ZeB_z(r_w - r_c)/m_Z$, B_z is the magnetic field, and r_c is the radial location of the guiding center of the gyro orbit. The step function in $f_\perp$ excludes ions whose gyro orbits would intersect the electrode wall. Note that at this point no attempt is made to remove from the ion phase space distribution those ions that will intersect the electrode wall due to the effect of a radial electric field.

Integration of the phase-space distribution function, $f(r,z,\mathbf{v}) = f_z(r,z,v_z) f_\perp(r,v_\perp)$, over all velocities under the guiding-center approximation, $r_c = r$, gives the ion density

$$\begin{aligned} n_Z(r,z) &= \int_{-\infty}^{\infty}\int_0^{\infty} f_z(r,z,v_z) f_\perp(r,v_\perp)\, dv_\perp\, dv_z \\ &= \frac{n_{0Z} e^{-\psi_i(r,z)+\psi_i(0,0)} (1 - e^{-\beta z [ZeB_z(r-r_w)/2]^2}) \operatorname{erfc}(\psi_m(r) - \psi(r,z)) \Theta(\mathbf{z}_m(r) - z)}{(1 - e^{-\beta_Z (ZeB_z r_w/2)^2}) \operatorname{erfc}(\psi_m(0) - \psi(0,0))}. \end{aligned} \tag{3}$$

Here n_{0Z} is the density of ions of charge state Z at the geometric center of the trap, and $z_m(r)$ is the location where the maximum potential occurs along a magnetic field line at r. Note that in the limit $B_z \to \infty$, no ions are ''scraped off'' by the wall, and the ion density at $z=0$ is radially constant out to the wall for each species.

For the electrons, the density profile is assumed to follow the Boltzmann relation axially at each radial position [3,5], $n_e(r,z) = n_e(r,0) e^{e[\phi(r,z) - \phi(r,0)]/T}$. To obtain a self-consistent solution for the electron and ion density profiles for $z>0$, a boundary condition $n_e(r,0)$ must be specified. Within the inner well, any radial electric field produced by the plasma due to a radial charge separation can be expected to cause radial diffusion. The effect, for $L_0 \gg L_1$, is that the plasma will tend to be neutral toward $z=0$. In consideration of this, $n_e(r,0)$ is chosen such that the plasma is neutral at $z=0$. Although $L_0/L_1 = 2.5$ is selected for an example calculation below, the results are expected to be even more representative of $L_0/L_1 > 2.5$. It should be emphasized that no attempt is made to model radial diffusion processes.

The finite difference algorithm used to solve Poisson's equation is based on the simultaneous overrelaxation numerical approach described in Ref. [6]. With the symmetry assumptions, the algorithm is implemented on a two-

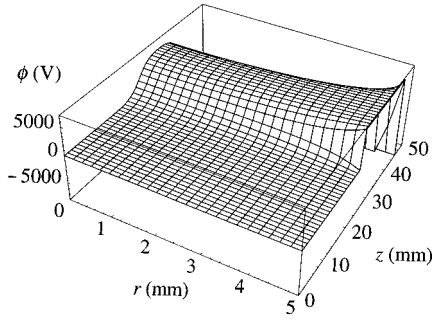

FIG. 2. Self-consistent electric potential. The calculation parameters are given in the text.

dimensional ($r>0$, $z>0$) grid. The grid spacing is selected to have at least two lattice points per Debye length as prescribed in Ref. [6]. For good convergence, the algorithm is run until the maximum change of potential per computation step is less than one part in 10^5 at a test lattice site ($r=0$, $z=\frac{1}{2}z_w$).

The charge state distribution of the ions is determined from the steady state corona model [7]. The corona model assumes an equilibrium resulting from the competing processes of collisional ionization and radiative recombination:

$$x^{+Z}+e\rightarrow x^{+(Z+1)}+e+e, \tag{4}$$

$$e+x^{+(Z+1)}\rightarrow x^{+Z}+\gamma, \tag{5}$$

where x^{+Z} is an ion of charge state $+Z$. This model is applicable to the low density, static plasma considered here. The charge state ratio predicted by this model is

$$\frac{N_Z}{N_{Z+1}}=7.87\times 10^{-9}\left(\frac{U_Z}{e}\right)^2\left(\frac{U_Z}{T_e}\right)^{3/4}e^{U_Z/T_e}, \tag{6}$$

where U_Z is the ionization potential of charge state Z, and $T_e=T$ is the electron temperature. Charge states that account for less than 0.1% of the ions are neglected by the algorithm. To keep the total number of ions constant, and the charge state distribution in agreement with the corona model, the central density n_{0Z} of each ion charge state is adjusted by the algorithm each time a selected number of computation steps pass.

An argon plasma having a temperature, $T=3$ keV, is used for the calculation. At this temperature only charge states $+16$ through $+18$ are followed. The charge spectrum is 24.1% charge state $+16$, 36.0% charge state $+17$, and 39.9% charge state $+18$. The average charge state is $+17.2$. Other values chosen for the calculation are the electrode dimensions, $r_w=0.5$ cm, $L_0=5$ cm, $L_1=2$ cm, and $L_2=0.5$ cm, and the electrode voltages $V_0=0$ V, $V_1=6.7$ kV, and $V_2=-82$ kV. The axial magnetic field B_z is chosen to be 10 T. The total number of trapped ions is 2.45×10^8, while the total number of trapped electrons is 7.24×10^{10}.

Figure 2 shows the electric potential resulting from both the externally applied voltages and the plasma's self-produced electric field. Along the wall, at $r=0.5$ cm, the potential profile is similar to the nested square well profile shown in Fig. 1(a). This occurs because the separations between electrodes are neglected. Along the center of the trap,

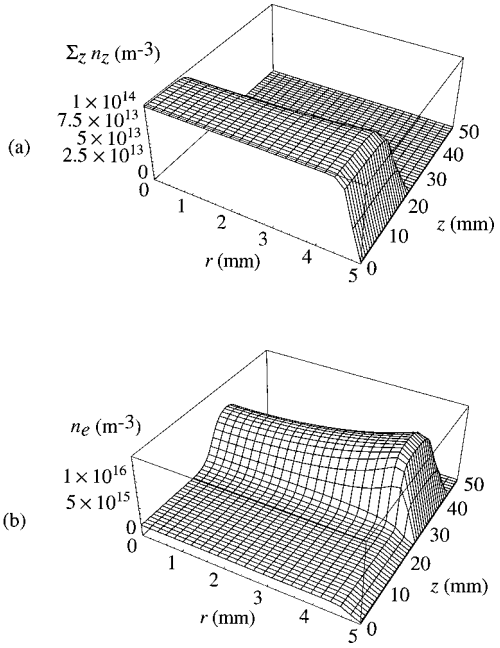

FIG. 3. Self-consistent ion and electron plasma densities. The total ion density profile (a) indicates the ions are trapped within the inner well, while the electron density profile (b) indicates the electrons are predominantly trapped within the end wells.

at $r=0$, the potential profile is much smoother, as expected. Inside the outer electrode, at $z\geqslant 4.5$ cm, the potential is off the scale in Fig. 2. Because of the large potentials and small gap (the grid spacing) between electrodes in the computational model, nonsustainable electric fields arise. Negligibly small gaps between electrodes are commonly used to reduce computation time and complexity [6,8–10]. An actual experiment will require some modification of the setup, including larger gaps between the electrodes.

Figure 3 shows the total ion density and the electron density. For $B_z=10$ T, the decrease in plasma density near the wall (due to intersection of the ion gyro orbits with the electrodes) is not appreciable except very close to the wall. The overlap of the ions in the inner well by the electron plasma neutralizes the space charge associated with the ions. A plot of the magnitude of the charge density, shown in Fig. 4, illustrates that most of the inner well region is neutral. The end-well region is non-neutral, however, as expected. In fact, the non-neutral plasma in an end well produces an electric field which is responsible for Debye shielding of the end

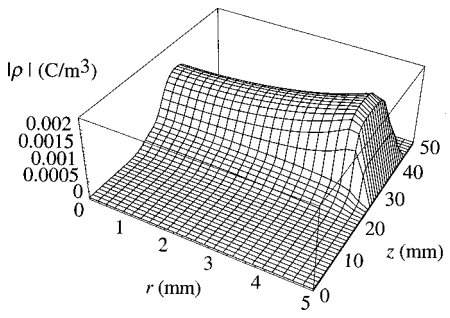

FIG. 4. Magnitude of the charge density. Note that the inner well region is neutral.

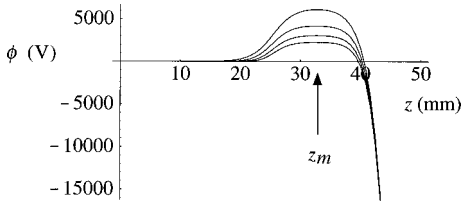

FIG. 5. Electric potential profile at $r=0$ for various plasma densities. The electric potential along the axis is shown for the case of no plasma (top curve) and three different plasma densities ($\Sigma_Z n_{0Z}=2.5\times10^{14}$, 5.0×10^{14}, $7.5\times10^{14}\,\mathrm{m}^{-3}$ for the next three lower curves, respectively).

well. As shown in Fig. 5, Debye shielding reduces the depth of the end well with increasing plasma density.

III. AXIAL CONFINEMENT

It is rather counterintuitive that a neutral plasma within a solenoidal magnetic field can be confined axially using a static electric field. To evaluate the axial transport properties of such a plasma, a variety of analytical approaches may be employed [11–22]. In the present work, the method used involves determining a phase-space distribution function that satisfies Vlasov's equation given a specified particle source boundary condition. The distribution function must additionally take into account inaccessible regions in phase space, and is only evaluated in one spatial dimension along a magnetic field line. (Hence no r dependence is considered in this section.) For the electrons, a source located at the maximum of the potential, $z=z_m$, is considered. The source emits electrons in the positive z direction having a Maxwellian velocity distribution. The corresponding electron phase-space distribution, normalized to the central electron density, is evaluated between z_m and z_w. It is

$$f_e(z,\mathbf{v})=n_{0e}\left(\frac{\beta_e}{\pi}\right)^{(3/2)} e^{-\beta_e v^2+\psi(z)-\psi(0)}\Theta(v_{me}+v_z), \quad (7)$$

where $v_{me}=[(\psi(z)-\psi(z_w))/\beta_e]^{1/2}$ is the minimum velocity in the positive z direction that allows an electron to reach z_w, $\beta_e=m_e/(2T)$, where m_e is the electron mass, and $\psi(z)=e\phi(z)/T$. The step function is included because electrons with a velocity in the z direction greater than v_{me} escape confinement. Therefore, no electrons can have a velocity in the negative z direction greater than v_{me} in the spatial region considered. Note that in the limit of perfect axial confinement, which occurs when $\psi(z_w)\to-\infty$ and $v_{me}\to\infty$, a Maxwell-Boltzmann phase-space distribution is approached.

Integrating f_e over velocity space, the electron density n_e is obtained for $z_m<z<z_w$:

$$n_e(z)=\tfrac{1}{2}n_{0e}e^{\psi(z)-\psi(0)}\,\mathrm{erfc}(-\sqrt{\psi(z)-\psi(z_w)}). \quad (8)$$

Integrating $v_z f_e$ over velocity space gives the net flux of electrons which escape confinement axially. The flux of electrons which escape confinement is constant for $z_m<z<z_w$, and is given by

$$F_e=\frac{n_{0e}e^{\psi(z_w)-\psi(0)}}{2\sqrt{\pi\beta_e}}. \quad (9)$$

With this, an axial confinement time scale can be defined as

$$\begin{aligned}\tau_e&=\frac{1}{F_e}\int_0^{z_w}n_e(z)dz\\&=\frac{1}{F_e}\left[\int_0^{z_m}n_{0e}e^{\psi(z)-\psi(0)}dz+\int_{z_m}^{z_w}\frac{1}{2}n_{0e}e^{\psi(z)-\psi(0)}\,\mathrm{erfc}(-\sqrt{\psi(z)-\psi(z_w)})dz\right]\\&=\sqrt{\pi\beta_e}e^{-\psi(z_w)}\left[2\int_0^{z_m}e^{\psi(z)}dz+\int_{z_m}^{z_w}e^{\psi(z)}\,\mathrm{erfc}(-\sqrt{\psi(z)-\psi(z_w)})dz\right].\end{aligned} \quad (10)$$

For simplicity, for $0<z<z_m$ the electrons are assumed to be in a Maxwell-Boltzmann phase-space distribution. The axial confinement time predicted by Eq. (9) is a lower bound. A plasma loses particles in the tails of the velocity distribution as considered here. However, these tails are not replenished instantaneously but at a finite rate by collisions or microinstabilities.

The minimum axial confinement time scale for ions is similarly calculated. A source of ions is considered at $z=0$, and ions which reach $z=z_m$ are considered lost from confinement. Thus

$$f_Z(z,\mathbf{v})=n_{0Z}\left(\frac{\beta_Z}{\pi}\right)^{3/2} e^{-\beta_Z v^2-Z(\psi(z)-\psi(0))}\Theta(v_{mZ}+v_z) \quad (11)$$

is the ion phase-space distribution for $0<z<z_m$. Here $v_{mZ}=[Z(\psi(z_m)-\psi(z))/\beta_z]^{1/2}$ is the minimum velocity in the positive z direction that allows an ion to reach z_m. Integration provides the ion density,

$$n_Z(z)=\tfrac{1}{2}n_{0Z}e^{-Z(\psi(z)-\psi(0))}\,\mathrm{erfc}[-\sqrt{Z(\psi(z_m)-\psi(z))}], \quad (12)$$

and the net axial flux of ions of charge state Z,

$$F_Z=\frac{n_{0Z}e^{-Z(\psi(z_m)-\psi(0))}}{2\sqrt{\pi\beta_Z}}. \quad (13)$$

The minimum axial ion confinement time scale is

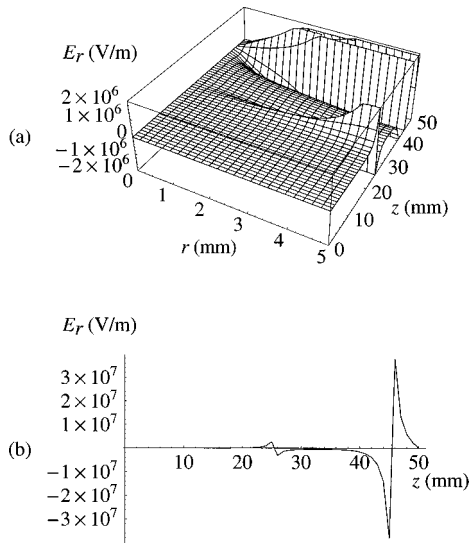

FIG. 6. (a) A plot of the radial component of the self-consistent electric field for the same parameters used in Figs. 2–4. (b) The radial component of the self-consistent electric field at r_w.

$$\tau_Z=\frac{1}{F_Z}\int_0^{z_m} n_Z(z)dz$$

$$=\sqrt{\pi\beta_Z}e^{Z\psi(z_m)}\int_0^{z_m} e^{-Z\psi(z)}$$

$$\times\operatorname{erfc}[-\sqrt{Z(\psi(z_m)-\psi(z))}]dz. \tag{14}$$

Because of geometric effects and plasma shielding, the electric potential along the $r=0$ magnetic field line is expected to provide the least axial ion confinement. Figure 5 illustrates this. Even without the plasma present the potential along the $r=0$ line only reaches a maximum of 6.4 kV, whereas along the electrode wall the maximum is 6.7 kV. For the self-consistent calculation of the axial electric potential profile in Sec. II (Figs. 2–4), the ion and electron minimum confinement times at $r=0$ are $\tau_Z\approx\tau_e\approx2$ h for $Z=+18$. These values are so large that each plasma component can be considered perfectly confined axially.

IV. RADIAL ION CONFINEMENT

In the absence of a radial electric field the trajectory of a particle in the trap will be a helix along a magnetic field line. With a radial electric field the trajectory becomes a superposition of a helical motion and an azimuthal $\mathbf{E}\times\mathbf{B}$ drift, provided the electric field is not too large. For a radial electric field which is proportional to r, an exact solution for the trajectory is possible [23]. However, as shown in Fig. 6, the self-consistent radial electric field for the nested-well trap is rather complex, and a numerical approach is required. Compared to electrons, ions have larger Larmor radii and, because they move slower, they are likely to reside longer within the electric field region which pulls them toward the wall. In the present section, the effect on the ions of the radial electric field produced by the voltage difference between the center electrode (at voltage V_0) and the first electrode (at voltage V_1) is considered. A Monte Carlo ion trajectory simulation is employed. All ions are considered to be

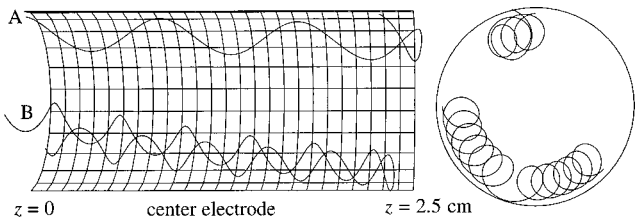

FIG. 7. Sample trajectories for ions in a uniform 10-T magnetic field and in the self-consistent electric potential shown in Fig. 2. (a) One trajectory results in radial escape, despite the fact that the initial gyro orbit does not intersect the wall. (b) For the other trajectory, the ion remains confined (just barely) for one pass.

argon with a charge state of $+17$. Ions start at $z=0$ with sampled values for r, v_z, and $v_\perp$ and the azimuthal direction of motion. Their trajectories are followed in three dimensions as they travel down the trap and back. The trajectory of each ion is solved for numerically assuming a uniform magnetic field (10 T) and using the electric potential that was self-consistently calculated in Sec. II. Some ions are pulled outward by the radially outward electric field and intersect the electrode walls. The program discards these particles and follows the others until they return to the $z=0$ plane. The initial velocity components are sampled from a Maxwellian distribution. The sampling equations used are

$$v_{zi}=\frac{\operatorname{erf}^{-1}(R_{1i})}{\sqrt{\beta_i}}, \tag{15}$$

$$v_{\perp i}=\sqrt{\frac{-\ln(R_{2i})}{\beta_i}}, \tag{16}$$

where R_{ni} is a uniformly distributed random number between 0 and 1. v_z is sampled from a half Maxwellian distribution such that only positive v_z values are generated. The azimuthal direction for $v_\perp$ is randomly chosen with a uniform distribution for all angles between 0 and 2π. An initial radial position is sampled using $r_i=r_w\sqrt{R_{3i}}$, which assumes an equally likely starting point anywhere within a circle of radius r_w. The Larmor radius r_L and initial radial location of the guiding center, r_c, are then calculated and any ion for which $r_c+r_L\geq r_w$ is discarded without actually solving for the trajectory to reduce computation time.

Figure 7 shows two sample ion trajectories, one which remains confined for one pass through the trap, and one which contacts the electrode wall. The initial conditions for the two trajectories are the same except that the escaping particle has an initial v_z that is twice that of the confined particle. The faster moving ion enters farther into the region with an appreciable radially outward electric field, and intersects the wall. Figure 8 shows the fraction of sampled orbits which remain confined, X_{conf}, for different radial positions. The results indicate that radial confinement is near perfect for one pass except very near the electrode wall. Overall, 94% of the ions remain confined for one pass. It should be noted that because the separation between electrodes is set equal to the grid spacing, the radial electric field created by the electrodes in the calculation is much larger than that

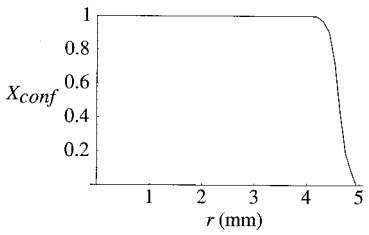

FIG. 8. The fraction of ions which remain confined for one pass vs initial radial position. The trajectories of 10 000 particles were followed.

which would occur in an actual trap. It can be concluded that the direct loss of ions due to the presence of a radially outward electric field can represent a reasonably small loss region in phase space.

V. CONCLUDING REMARKS

Because of the presence of an axial transition in neutrality, the plasma will experience a sheared azimuthal $\mathbf{E}\times\mathbf{B}$ flow. An interesting question is whether the sheared flow will inhibit or promote instabilities and anomalous transport processes. Such a question is highly relevant to other magnetic confinement configurations including tandem mirrors, tokamaks, and Z pinches [24–29]. At a minimum, the sheared azimuthal drift can be expected to apply a collisional torque between the neutral and nonneutral regions. With an ion mass nearly five orders of magnitude larger than the electron mass, the collisional torque should primarily affect the electron plasma. Hence radial diffusion is possible, and can be expected within the nonneutral electron plasma region. In addition, the neutral plasma will, given sufficient time, be able to diffuse across the magnetic field and form a plasma sheath adjacent to the inner surfaces of the electrodes. If partially stripped ions are confined, ionization and recombination processes may enhance radial ion diffusion. However, because a solenoidal magnetic field is used, cross-field transport processes in the neutral region may be slow relative to the anomalously fast transport processes that are observed in, for example, toroidal plasma confinement devices. In fact, experiments using solenoidal magnetic confinement indicate that cross-field transport, at least in non-neutral plasmas, can be understood with recently developed theory [30]. It will be interesting to see if the same is true for neutral plasmas.

Open magnetic field line approaches to confining neutral plasmas (e.g., tandem mirrors) generally have axial particle and energy loss rates that are larger than radial loss rates. The ability to provide near perfect axial confinement with the nested-well approach is advantageous in comparison. In addition, it may even be possible to achieve near perfect radial confinement using a rotating electric field confinement technique [31]. A rotating field could be applied to a non-neutral end-well region to confine the electron plasma radially. This should set up a radial electric field within the inner well that tends to radially confine the ion plasma so that the overlap region remains neutral. With the plasma well isolated from material surfaces, plasmas confined using the nested-well approach can be of very high purity, and can be associated with lower neutral gas pressures. In addition, a smaller plasma heating power is required with better confinement. It should be noted that the nested-well confinement technique could readily be used as a plug for a magnetic mirror.

A thermal, neutral, high-charge-state plasma confined in a nested-well trap appears well suited for studies of fundamental plasma processes under highly controlled conditions. In particular, studies on cross-field transport and on recombining plasmas can be useful for understanding magnetic plasma confinement and x-ray emission processes in plasmas. Cross-field transport studies can be performed on neutral plasmas or partially non-neutral rotating and/or sheared-flow plasmas using a straight solenoidal magnetic field, a curved field (e.g., one that forms half a toroid), or a magnetic mirror field. Studies on recombining high-charge-state plasmas can provide information on spontaneous and stimulated x-ray emission processes.

ACKNOWLEDGMENT

This material is based upon work supported by the National Science Foundation.

[1] T. M. O'Neil, in Non-Neutral Plasma Physics, edited by C. W. Roberson and C. F. Driscoll, AIP Conf. Proc. No. 175 (AIP, New York, 1988), p. 1; see also T. M. O'Neil, Phys. Today **52** (2), 24 (1999).
[2] D. S. Hall and G. Gabrielse, Phys. Rev. Lett. **77**, 1962 (1996).
[3] C. A. Ordonez, Phys. Plasmas **4**, 2313 (1997).
[4] C. A. Ordonez, IEEE Trans. Plasma Sci. **24**, 1378 (1996).
[5] C. F. Driscoll, J. H. Malmberg, and K. S. Fine, Phys. Rev. Lett. **60**, 1290 (1988).
[6] R. L. Spencer, S. N. Rasband, and R. R. Vanfleet, Phys. Fluids B **5**, 4267 (1993).
[7] R. W. P. McWhirter in Plasma Diagnostic Techniques, edited by R. H. Huddlestone and S. L. Leonard, (Academic, New York, 1965) p. 201.
[8] S. A. Prasad and T. M. O'Neil, Phys. Fluids **22**, 278 (1979).
[9] A. J. Peurrung and J. Fajans, Phys. Fluids B **2**, 693 (1990).
[10] R. L. Spencer and G. W. Hart, Phys. Fluids B **4**, 3507 (1992).
[11] K. Kurihara, Y. Kiwamoto, T. Saito, K. Yatsu, and S. Miyoshi, J. Phys. Soc. Jpn. **61**, 3153 (1992).
[12] T. Saito, Y. Kiwamoto, K. Kurihara, T. Cho, M. Inutake, S. Miyoshi, T. Tamano, and K. Yatsu, Phys. Fluids B **5**, 866 (1993).
[13] Y. Tatematsu, Y. Kiwamoto, T. Saito, and T. Tamano, J. Phys. Soc. Jpn. **63**, 558 (1994).
[14] Y. Tatematsu, Y. Kiwamoto, T. Saito, Y. Yoshimura, T. Takahashi, I. Katanuma, M. Inutake, and T. Tamano, J. Nucl. Mater. **220–222**, 575 (1995).
[15] T. Saito, Y. Kiwamoto, Y. Tatematsu, Y. Yoshimura, T. Takahashi, M. Inutake, and T. Tamano, Phys. Plasmas **2**, 352 (1995).
[16] L. A. Schwager and C. K. Birdsall, Phys. Fluids B **2**, 1057 (1990).

[17] L. A. Schwager, Phys. Fluids B **5**, 631 (1993).
[18] C. A. Ordonez, Phys. Fluids B **4**, 778 (1992).
[19] C. A. Ordonez, Phys. Rev. E **55**, 1858 (1997).
[20] R. H. Cohen, M. E. Rensink, T. A. Cutler, and A. A. Mirin, Nucl. Fusion **18**, 1229 (1978).
[21] R. H. Cohen, I. B. Bernstein, J. J. Dorning, and G. Rowlands, Nucl. Fusion **20**, 1421 (1980).
[22] V. N. Khudik, Nucl. Fusion **37**, 189 (1997).
[23] R. C. Davidson, Theory of Nonneutral Plasmas (Benjamin, Reading, MA, 1974) p. 9.
[24] H. L. Berk, M. N. Rosenbluth, R. H. Cohen, and W. M. Nevins, Phys. Fluids **28**, 2824 (1985).
[25] J. A. Byers and R. H. Cohen, Phys. Fluids **28**, 1589 (1985).
[26] J. A. Byers, Phys. Fluids **29**, 1547 (1986).
[27] R. H. Cohen, W. M. Nevins, and H. L. Berk, Phys. Fluids **29**, 1578 (1986).
[28] K. H. Burrell, Science **281**, 1816 (1998).
[29] U. Shumlak and C. W. Hartman, Phys. Rev. Lett. **75**, 3285 (1995).
[30] D. H. E. Dubin, Phys. Plasmas **5**, 1688 (1998).
[31] F. Anderegg, E. M. Hollmann, and C. F. Driscoll, Phys. Rev. Lett. **81**, 4875 (1998).